Journal of Materials Chemistry C

RSC Publishing

PAPER

View Article Online
View Journal | View Issue

Single crystal biphenyl end-capped furan-incorporated oligomers: influence of unusual packing structure on carrier mobility and luminescence†

Cite this: *J. Mater. Chem. C*, 2013, **1**, 4163

Kazuaki Oniwa,[a] Thangavel Kanagasekaran,[a] Tienan Jin,*[a] Md. Akhtaruzzaman,[b] Yoshinori Yamamoto,[ac] Hiroyuki Tamura,[a] Ikutaro Hamada,[a] Hidekazu Shimotani,[d] Naoki Asao,[a] Susumu Ikeda*[a] and Katsumi Tanigaki*[a]

Received 2nd February 2013
Accepted 26th April 2013

DOI: 10.1039/c3tc30220b

www.rsc.org/MaterialsC

We report the synthesis and characterization of two new furan-based biphenyl end-capped oligomers, 2-([1,1′-biphenyl]-4-yl)-5-(5-([1,1′-biphenyl]-4-yl)thiophen-2-yl)furan (BPFT) and 5,5′-di([1,1′-biphenyl]-4-yl)-2,2′-bifuran (BP2F) as candidate semiconductors for organic light-emitting field effect transistors (OLETs). Differential scanning calorimetry (DSC) and thermogravimetric analysis (TGA) showed the high thermostability of these furan-based semiconductors. X-Ray crystallography of single crystals grown by physical vapor transfer (PVT) method revealed a complicated herringbone packing of BPFT stacking with unusual flat and bent structures, which is different from that of BP2F and the bithiophene-based analogue 5,5′-di([1,1′-biphenyl]-4-yl)-2,2′-bithiophene (BP2T). BPFT single crystal showed a higher absolute quantum yield (51%) compared to that of BP2F and BP2T. Density Functional Theory (DFT) calculations showed that the different excitation energies between flat and bent structures led to the asymmetric transition dipoles in dark state of BPFT H-aggregates, which explains the highest PLQY of BPFT single crystal. Single crystal FET based on BPFT showed an ambipolar characteristic with high hole and electron mobilities, while single crystal FET based on BP2F exhibited p-type characteristic with a high hole mobility. Light emission was observed from the single-crystal FET based on BPFT.

Introduction

Furan-based organic semiconductors are of increasing interest in organic electronics,[1–4] even though they have attracted far less attention than the well-known thiophene analogues due to the lower stability of furan in oxidative conditions.[5] Recent advances on furan-based organic semiconductors in device applications including organic field-effect transistors (OFETs),[2] organic light-emitting diode (OLEDs),[3] and organic photovoltaics (OPVs),[4] demonstrated their sufficient stability, high carrier mobility and more efficient fluorescent property than thiophene analogues. Although the p-type field-effect characteristic of those materials such as oligofurans, limited the electron injection to generate exciton results weak emission intensity,[2c] these observations implied the potential application opportunities of the furan-based semiconductors in organic light-emitting field effect transistors (OLETs).

OLETs are one of the most promising multifunctional devices that combine both switching properties of transistors and the emission capability of LEDs in a simple device.[6–9] OLETs require the materials to possess both high carrier mobility and high photoluminescence quantum yields (PLQYs) to realize the potential applications in active matrix full color display and electrically driven organic laser.[6b] However, in most cases, organic semiconductors with high carrier mobility obtained from the strong intermolecular π–π stacking lead to luminescence quenching in the solid state due to the singlet fission or exciton quenching. For examples, rubrene, tetracene, and pentacene exhibited superior FET mobility but they have low or no emission,[10] while the PLQYs are *vice versa*.[11] Nevertheless, most recently the maximized charge mobility and the absolute PLQY have been achieved by Perepichka and co-workers using 2-(4-hexylphenylvinyl)anthracene (HPVAnt) as an OLET material in the crystalline state.[8] An alternative candidate for OLET materials is thiophene/phenylene co-oligomers, which possess high luminescence efficiency and ambipolar FET behavior.[9] For example,

[a]*WPI-Advanced Institute for Materials Research (WPI-AIMR), Tohoku University, Sendai, 980-8577, Japan. E-mail: tjin@m.tohoku.ac.jp; sikeda@m.tohoku.ac.jp; tanigaki@sspns.phys.tohoku.ac.jp; Fax: +81-22-217-5979; Tel: +81-22-217-6177*

[b]*Department of Chemistry, Faculty of Science, University of Malaya, 50603, Kuala Lumpur, Malaysia*

[c]*State Key Laboratory of Fine Chemicals, Dalian University of Technology, Dalian, 116012, P. R. China*

[d]*Graduate School of Science, Department of Physics, Tohoku University, Sendai, 980-8577, Japan*

† Electronic supplementary information (ESI) available: Thin film OFET characterizations, theoretical calculation data, and crystal data. CCDC 922141 and 922142. For ESI and crystallographic data in CIF or other electronic format see DOI: 10.1039/c3tc30220b

recently we reported that FETs based on 5,5′-di([1,1′-biphenyl]-4-yl)-2,2′-bithiophene (BP2T) single crystal showed high ambipolar carrier mobility and strong edge emission.[9b] However, in the preliminary measurements, we observed that BP2T single crystal has a moderate PLQY of 38% (*vide infra*). Considering that, materials containing oxygen atom which has a smaller van der Waals radius than sulfur atom may lead to closer packing structures, and in terms of efficient fluorescent property of oligofurans,[1] we envisioned that the partial or full replacement of sulfur to oxygen in BP2T will supply the elevated materials with both increased carrier mobility and luminescence efficiency. We report here on the synthesis, characterization, implementation in OFETs, and light-emitting behavior of two new biphenyl end-capped furan-incorporated oligomers based on 2-([1,1′-biphenyl]-4-yl)-5-(5-([1,1′-biphenyl]-4-yl)thiophen-2-yl)furan (BPFT) and 5,5′-di([1,1′-biphenyl]-4-yl)-2,2′-bifuran (BP2F) (Scheme 1). Interestingly, the new BPFT single crystal containing thienylfuran moiety showed two different flat and bent structures which stack with each other in a herringbone manner. OFETs based on BPFT show an ambipolar characteristic with a higher absolute PLQY of 51% than that of BP2T and BP2F in the crystalline state.

Results and discussion

Synthesis and characterization

As shown in Scheme 1, BPFT was synthesized by dibromination of 2- and 2′-positions of 2-(2′-thieno)furan followed by the double Suzuki–Miyaura coupling with biphenyl boronic acid in high yield. BP2F was prepared through Suzuki–Miyaura coupling of 2-furanyl boronic acid with 4-bromo-1,1′-biphenyl followed by copper-mediated homo-coupling of the lithiated resulting 2-[(1,1′-biphenyl)-4-yl]furan. These three materials were purified by thermal sublimation under reduced pressure for 2 times due to their poor solubility in common organic solvents. The structures of BPFT and BP2F were determined by elemental analysis and X-ray crystallography. Among the differential scanning calorimetry (DSC) measurements, BPFT showed the lowest melting points of 297 °C compared to BP2F (321 °C) and BP2T (370 °C). The thermogravimetric analysis (TGA) revealed that a 10% weight was lost at 445, 413, and 398 °C for BP2T, BPFT, and BP2F, respectively. The DSC and TGA results revealed the high thermal stability of the furan-based new materials BPFT and BP2F (Fig. 1).

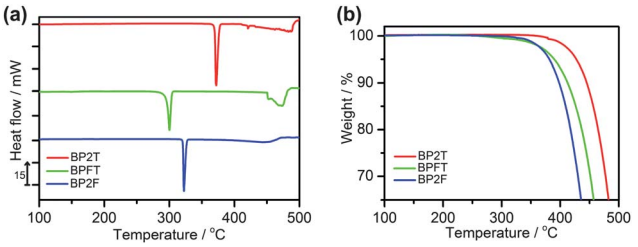

Fig. 1 DSC (a) and TGA (b) of BP2T, BPFT and BP2F.

Single crystal structures

Single crystals of the three materials were grown by a physical vapor transport (PVT) method under argon gas atmosphere. Single crystals of BP2T and BPFT were obtained as a lamella shape, whereas BP2F showed a needle-like single crystal.[12] The crystal packing structures and conformations were determined by means of X-ray crystallography. As shown in Fig. 2a and b, BP2F in single crystals stack in a slipped herringbone manner with a completely flat structure, and BPFT shows a herringbone structure similar to that of BP2T with the long axes of molecules oriented in parallel with the herringbone angle of 59°. It is interesting that BPFT exhibited a more complicated herringbone packing arrangement than BP2T and BP2F due to its unusual two molecular geometries, flat and bent structures. BPFT displayed an alternate flat–bent packing along the *z* axis and flat–flat as well as bent–bent parallel packing along *x* axis (Fig. 2e and f). As a result, the intermolecular distances (d_1 *vs.* d_4, d_2 *vs.* d_5, d_3 *vs.* d_6) between those adjacent molecules in BPFT from both the thiophene side and the furan side are totally different; the shortest and the longest distances were shown to

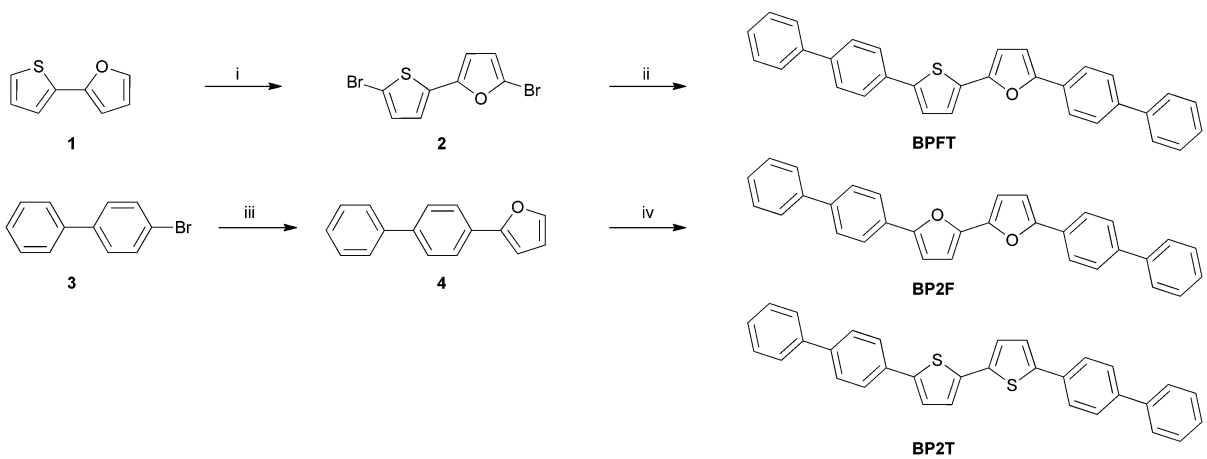

Scheme 1 Synthesis of BPFT and BP2F as well as the structure of BP2T. *Reaction conditions*: (i) NBS, CH_2Cl_2, rt, ultrasound, 5 min. (ii) 1,1′-Biphenyl-4-yl boronic acid, $Pd(P^tBu_3)_2$, KF, THF, rt. (iii) Furan-2-yl boronic acid, $Pd(P^tBu_3)_2$, KF, THF, rt. (iv) *n*-BuLi, $CuCl_2$, THF, −78 °C to rt.

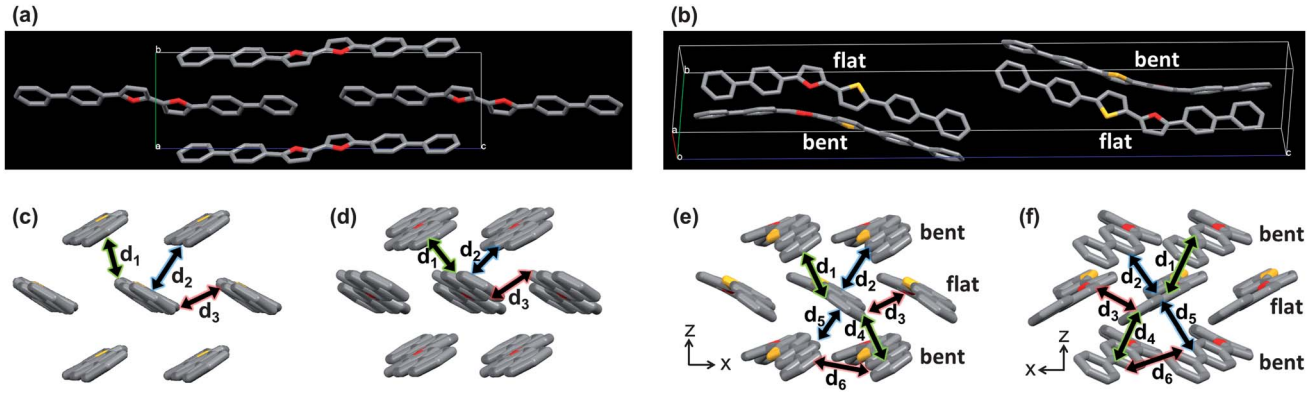

Fig. 2 Packing structures of (a) slipped herringbone packing with flat structure of BP2F, (b) herringbone packing with flat and bent structures of BPFT, and intermolecular distances of (c) BP2T, (d) BP2F, (e) BPFT from thiophene side, (f) BPFT from furan side. Hydrogen atoms are omitted for clarity. Red: oxygen atom, yellow: sulfur atom.

Table 1 Summarized intermolecular distance (Å)

		BPFT		
	BP2T	S-side[a]	O-side[b]	BP2F
d_1	3.69	3.64	3.54	3.63
d_2	3.71	3.60	3.62	3.60
d_3	3.84	3.88	3.65	3.64
d_4	—	3.60	3.74	—
d_5	—	3.54	3.79	—
d_6	—	3.91	3.61	—

[a] Thiophene side of BPFT. [b] Furan side of BPFT.

Table 2 Summarized optical properties

	$CHCl_3$ solution			Single crystal	
	λ_{abs} (nm)	λ_{em}[a] (nm)	Φ_f[b] (%)	λ_{em}[c] (nm)	Φ_f[b] (%)
BP2T	390	456, 481	25	587	38
BPFT	393	448, 474	40	549	51
BP2F	386	431, 455	80	516	37

[a] Excitation wavelength is 390 nm for all compounds. [b] Absolute quantum yield determined by integrating sphere system. Φ_f: photoluminescence quantum yield. [c] Excitation wavelength: 420 nm for BP2T, 380 nm for BPFT, 350 nm for BP2F.

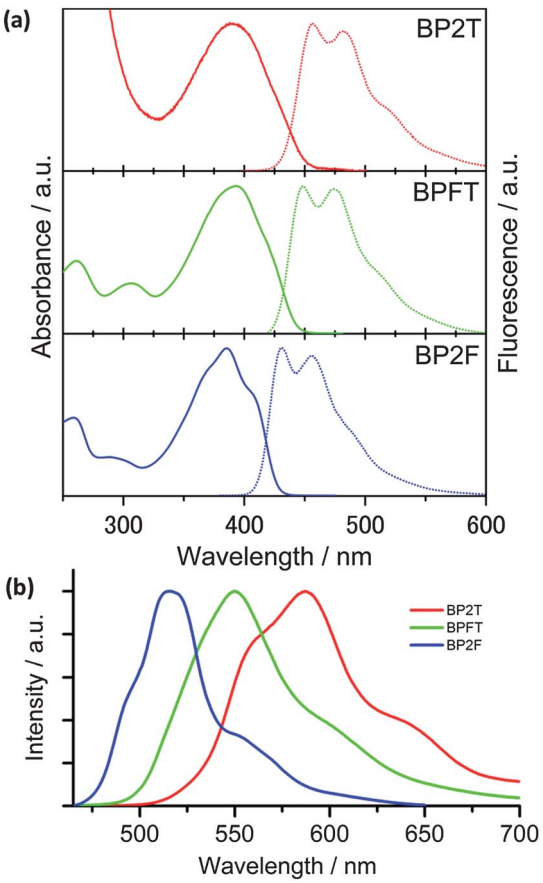

Fig. 3 Optical properties of BP2T, BPFT, and BP2F. (a) Absorption (solid line) and fluorescent (dot line) spectra in $CHCl_3$ and (b) photoluminescence spectra in the crystalline state.

be 3.54 Å and 3.91 Å, respectively (Table 1). These clear differences between BPFT and BP2F or BP2T in crystal structures might be ascribed to the asymmetric structure of BPFT which has the different ring size of thiophene and furan. The average intermolecular distance of 3.67 Å in BPFT and the shortest distance of 3.60 Å in BP2F are shorter than in BP2T (3.69 Å) (Fig. 2c and d, Table 1),[13] indicating the tighter packing structures of BPFT and BP2F than that of BP2T. This result is consistent with the trend in oligofurans and oligothiophenes. We expected that the packing mode differences between BPFT, BP2F, and BP2T in crystalline state may exhibit distinct optoelectronic and FET properties.

Optical property

Optical properties of the three materials were characterized in chloroform solution and in crystalline state, respectively, as summarized in Table 2. As shown in Fig. 3a, the UV/vis spectra of the three compounds in chloroform showed almost similar absorption maxima (λ_{max}) in the range of 386–393 nm. In contrast, the clear blue-shifts of emission maxima (λ_{em}) of BPFT

Table 3 OFET performances of BP2T, BPFT, and BP2F in single crystals[a]

	μ_h	V_{th} (V)	μ_e	V_{th} (V)
BP2T	0.08	−60	0.011	92
BPFT	0.27	−45	0.013	94
BP2F	0.32	−7	—[b]	—[b]

[a] PMMA was used as insulator on SiO_2 substrate. [b] Not observed. V_{th}: threshold voltage; μ_h: hole mobility; μ_e: electron mobility; I_{on}/I_{off}: current on/off ratios.

and BP2F were observed compared to BP2T. The smaller stokes shift in the furan-based molecules indicates that BPFT and BP2F structures are more rigid than BP2T due to their more quinoid structural characteristics. PLQY (Φ_f) for BP2F in solution is very high (80%) whereas the lower values were observed for BPFT (40%) and BP2T (25%), suggested the significant furan effect on photoluminescence property. This quantum yield enhancement can be explained by the decreased heavy atom effect from sulfur to oxygen atom and the more molecular rigidity of BP2F and BPFT relative to BP2T.

The fluorescence spectra of the three materials in the crystalline state showed a significant red-shift compared to that in solution, implying that the energy gap of band structures between the valence and conduction band caused by single crystals with a highly ordered molecular packing, is smaller than the HOMO–LUMO gap in the single molecule (Table 2 and Fig. 3b). In addition, the blue shift of BPFT and BP2F compared to BP2T explains their stronger π–π interaction in the single crystals. The absolute PLQYs in crystalline state were measured in an integrating sphere. The higher PLQY of 51% was observed for single crystal BPFT than that for BP2F (37%) and BP2T (38%) (Table 1). Time dependent density functional theory (TD-DFT) calculations using B3LYP/6-31G++(d,p) as an exchange-correlation functional and basis set showed that the energies of singlet exciton (S_1) are 2.63 eV for BP2T, 2.69 eV for BPFT, and 2.77 eV for BP2F, respectively (Table S2†). The energies of the two triplets (T_1) of the three compounds were calculated to be in the range of 1.66–1.85 eV, which are unfavorable for generating singlet fission ($S_1 < 2T_1$).[8,10] We also evaluated excitation energy and transition dipole moment by TDDFT from their aggregates (Table S3†).[14] Although the opposite transition dipole cancels out in the dark state of the BP2T H-aggregates which takes ordinary herringbone packing, the transition dipole does not completely cancel out in the dark state of the BPFT H-aggregates consisting of the bent and flat molecules. This is due to the exciton population in BPFT the flat molecules tend to be larger than at the bent molecules because of the lower excitation energy of flat molecules than that of bent molecules; 2.93 eV for flat BPFT and 2.98 eV for bent BPFT (Table S4†).[14] This calculation may explain the reason why the PLQY of BPFT crystal is higher than that of BP2T, even though the transition dipole moments of the BP2T and BPFT single molecules are similar. In addition, despite the existence of bifuranyl moiety, the PLQY of single crystal BP2F showed a similar fluorescent efficiency to that of BP2T, which is ascribed to the strong π–π interaction of

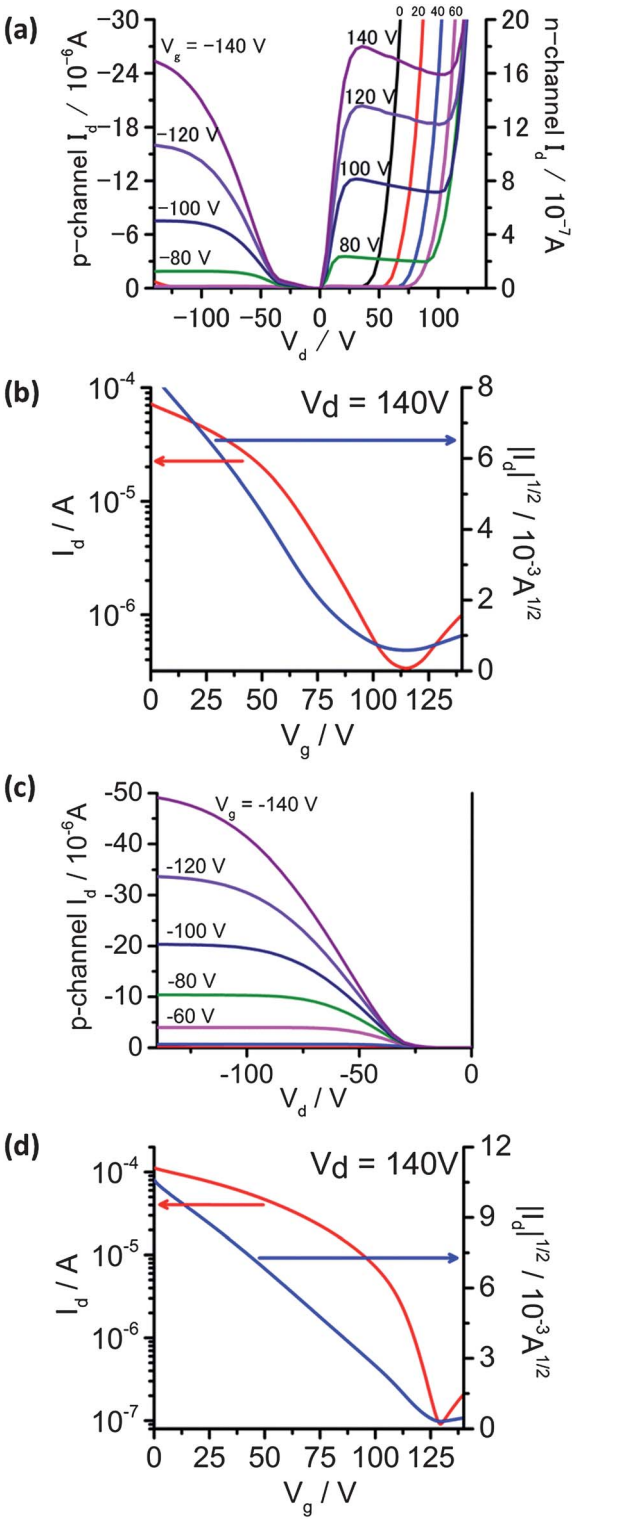

Fig. 4 Output (a) and transfer (b) characteristics of BPFT-based SC-FETs, output (c) and transfer (d) characteristics of BP2F-based SC-FETs.

BP2F in crystalline state as mentioned in Fig. 3. These results indicate that a slight modification from bithiophene to thienylfuran or bifuran skeleton in a molecule leads to a dramatic difference in the optical properties due to the varied packing arrangement and the decreased heavy atom effect.

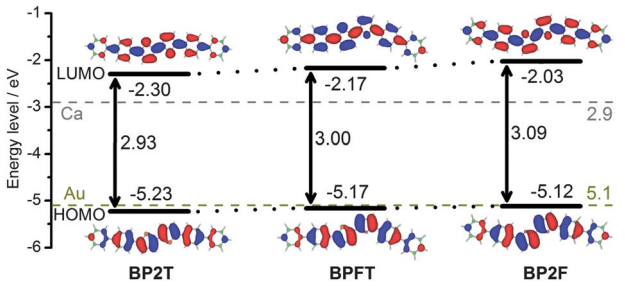

Fig. 5 Energy diagram of frontier orbitals calculated by DFT at the B3LYP/6-31G++(d,p).

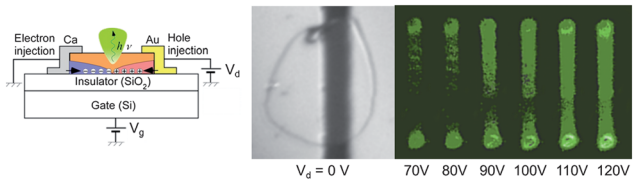

Fig. 6 Light emitting behavior of BPFT-based SC-FET.

OFET performances

FET properties based on these compounds were investigated in thin films and single crystals in bottom-gate and top-contact configuration. The thin film transistors (TFTs) were fabricated by vacuum deposition of organic semiconductors on the surface of PMMA pre-treated SiO_2 substrate with gold as source and drain electrodes (Fig. S1†). TFTs based on the three compounds showed only p-type behavior, and the slightly increased hole mobility was observed in BPFT (0.031 $cm^2 V^{-1} s^{-1}$) and BP2F (0.047 $cm^2 V^{-1} s^{-1}$) compared to that in BP2T (0.023 $cm^2 V^{-1} s^{-1}$) under similar conditions (Table S7†).

Single crystal FETs (SC-FETs) were also fabricated using Au and Ca as the source and drain electrodes. Single crystals grown by PVT method were electrostatically laminated on PMMA pre-treated SiO_2 substrate. The single crystal BPFT behaves as an ambipolar semiconductor as shown in the output and transfer characteristic curves in Fig. 4a, b and S3.† The hole and electron mobility were extracted to be 0.27 $cm^2 V^{-1} s^{-1}$ and 0.013 $cm^2 V^{-1} s^{-1}$, respectively, by analysing the saturation region (Table 3). The hole mobility of BPFT device was higher than that in BP2T device (0.08 $cm^2 V^{-1} s^{-1}$ for hole, Fig. S2†) and the electron mobilities of both devices were almost similar. The threshold voltages (V_{th}) of BPFT device in p and n modes were deduced to be −45 V and 94 V. It should be noted that, the steep increase in n-channel drain current at high drain voltage indicates the onset of hole transport as shown in Fig. 4a. However, the analogous electron current is almost invisible in p-channel drain current because of the much lower electron current than the hole current. Moreover, the unusual shape of the electron current in n-channel compared to the p-channel in the output characteristic of Fig. 4a might be attributed to the time-dependent electron-current decay as a result of the high applied gate voltage. The similar phenomenon was also observed in other ambipolar SC-FETs, such as BP3T.[9a] In the case of SC-FET based on BP2T (Fig. S2†), the similar phenomenon might be exhibited if the drain voltages are more than 140 V. The difference between BPFT and BP2T should be related to the lower threshold voltage (V_{th}) of BPFT than that of BP2T for holes (45 V *vs.* 60 V, Table 3). SC-FETs based on BP2F exhibited only p-type characteristic; the hole mobility increased up to 0.32 $cm^2 V^{-1} s^{-1}$ due to the closed packing structure of BP2F single crystal (Fig. 4c and d). The charge transfer integrals (t) among HOMOs and LUMOs were calculated on the basis of the crystal structures to evaluate the experimental carrier mobility (Table S6†).[15] The maximum t values among HOMOs for BP2T, BPFT, and BP2F in dimers were showed to be 45.0, 40.5, and 59.4 meV, while the maximum t values among LUMOs were 127.4, 94.9, and 66.7 meV, respectively. BP2F bearing bifuran unit exhibited the highest transfer integrals among HOMOs, suggesting its highest hole mobility which is in agreement with the experimental result. Furthermore, the higher t values of BP2T and BPFT than that of BP2F among LUMOs indicated their ambipolar behavior. Moreover, the ratio of maximum and minimum t values among HOMOs for BPFT is about 30 (40.5 meV *vs.* 1.4 meV), while the ratio is about 4 for BP2T (45.0 meV *vs.* 12.8 meV), suggesting the much higher anisotropy for BPFT than that for BP2T. The replacement of thiophene to furan in these biphenyl end-capped oligomers did not show significant reorganization energy differences; the almost similar reorganization energies for hole (0.21–0.22 eV) and electron (0.20–0.21 eV) formation in the three materials were calculated (Table S5†).

HOMO and LUMO energy calculations

Theoretical calculations revealed that both HOMO and LUMO levels of BPFT and BP2F, as well as their band gaps increased by the introduction of furan ring (Fig. 5). The increased band gaps are ascribed to the much increased LUMO levels of BPFT and BP2F due to the wave function of LUMO localized on hetero atoms. As a result, the introduction of furan moiety enhanced the p-type FET characteristic due to the decreased hole injection barrier between gold electrode (work function = 5.1 eV) and HOMO, as well as the increased electron injection barrier between calcium electrode (work function = 2.9 eV) and LUMO.

Light emission SC-FETs

The emission was observed from the SC-FET based on BPFT single crystal. Fig. 6 shows a series of light-emitting FET device top images with various drain voltage (V_d) between 70 V and 120 V at a fixed gate voltage (140 V). The clear light emission appeared from the edge of single crystal BPFT at low V_d regime. The intensity of the emission increased with increasing V_d. We note that the similar light-emitting behavior of SC-FET based on BP2F was not observed.

Conclusion

In conclusion, we have disclosed that a new series of furan-based BPFT and BP2F showed distinct optoelectronic and FET properties relative to the thiophene analogue BP2T material. The PLQY of BPFT crystal is higher than that of BP2T and BP2F due to the unusual packing arrangement of BPFT consisting of flat and bent structures, even though BPFT has a more dense packing structure than that of BP2T. Our DFT calculations showed that the different excitation energy between flat and bent structures led to the asymmetric transition dipoles in dark state of BPFT H-aggregates, which explains the highest PLQY of BPFT single crystal. OFET based on BPFT exhibited an ambipolar characteristic, while BP2F showed a unipolar behavior with a high hole mobility. The bright light emitting FET was observed upon the applied drain voltage demonstrating the good electroluminescent efficiency of BPFT single crystal. This observation provides a promising strategy to develop new OLET materials which possess both high photoluminescence efficiency and charge mobility.

Experimental

General information

^{1}H NMR and ^{13}C NMR spectra were recorded on JEOL JNM AL 400 (400 MHz) spectrometers. ^{1}H NMR spectra are reported as follows: chemical shift in ppm (δ) relative to the chemical shift of $CDCl_3$ at 7.26 ppm, integration, multiplicities (s = singlet, d = doublet, t = triplet, q = quartet, m = multiplet and br = broadened), and coupling constants (Hz). ^{13}C NMR spectra were recorded on JEOL JNM AL 400 (100.5 MHz) spectrometers with complete proton decoupling, and chemical shift reported in ppm (δ) relative to the central line of triplet for $CDCl_3$ at 77 ppm. UV/vis absorption spectra were recorded on a JASCO V-650DS spectrometer. Fluorescence spectra were recorded on a HITACHI F-7000 spectrophotometer and absolute fluorescence quantum yields were measured by a photon-counting method using an integration sphere on a Hamamatsu Photons C9920-02 spectrometer. Elemental analyses were measured on J-SCIENCE Lab JM-10 and YANAKO HNS-ah/HSU-20 in Research and Analytical Center for Giant Molecules, Tohoku University. DSC was measured by a RIGAKU DSC8230 using N_2 atmosphere at a scan rate of 10 K min^{-1}. TGA was measured by a RIGAKU TAG8120. X-Ray analysis was carried out at −180 °C with a Rigaku VariMax with RAPID diffraction by using graphite monochromated Cu-Kα radiation. The structures were solved by direct method. Column chromatography was carried out employing silica gel 60 N (spherical, neutral, 40–100 μm, KANTO Chemical Co.). Analytical thin-layer chromatography (TLC) was performed on 0.2 mm precoated plate Kieselgel 60 F254 (Merck). Single crystals of BP2T, BPFT, and BP2F were grown by a physical vapor transport (PVT) method under argon gas atmosphere using a separation temperature controller (AMF-9P-III, ASAHI RIKA).

Materials

The commercially available compounds were used as received. The BP2T was purchased from Kanto Chemical Co., Inc., and 2-(2-thienyl)furan (**1**) was purchased from Aldrich. Single crystals of BP2T, BPFT, and BP2F were grown by PVT method, and the structures of BPFT and BP2F were determined by elemental analysis and X-ray crystallography.

Synthesis of 2-bromo-5-(5-bromothiophen-2-yl)furan (2)

A mixture of 2-(thiophen-2-yl)furan (**1**) (1 mmol, 150 mg) and *N*-bromosuccinimide (2 mmol, 365 mg) in CH_2Cl_2 (15 mL) was subjected to ultrasonic irradiation for 3 min at rt. Reaction mixture was purified by florisil column chromatography (eluent : hexane), giving the corresponding 2-bromo-5-(5-bromothiophen-2-yl)furan (**2**) in 98% (300 mg) yield as a yellow oil. ^{1}H NMR (400 MHz, $CDCl_3$): δ 6.97 (d, J = 4.4 Hz, 1H), 6.96 (d, J = 4.4 Hz, 1H), 6.39 (d, J = 3.2 Hz, 1H), 6.34 (d, J = 3.2 Hz, 1H); ^{13}C NMR (100 MHz, $CDCl_3$): δ 150.09, 133.90, 130.44, 122.88, 121.38, 113.39, 111.63, 107.60.

Synthesis of BPFT

To a mixture of 4-biphenylboronic acid (4 equiv., 2.61 g), Pd[P(*t*-Bu_3)]$_2$ (2 mol%, 40 mg), KF (1.5 g) was added the 2-bromo-5-(5-bromothiophen-2-yl)furan (**2**) (3.3 mmol, 1.02 g) in THF (20 mL) solution under N_2 atmosphere. The reaction mixture was stirred for 12 h at rt. To the reaction mixture was added MeOH (10 mL) and the resulting residue was filtered by washing with water and MeOH. The residue was further purified by sublimation at 300 °C (yellow solid; 1.30 g, 87%). Anal. calcd for $C_{32}H_{22}OS$: C 84.55, H 4.88, O 3.52, S 7.05; found: C 84.60, H 5.09, S 7.04%.

Synthesis of 2-([1,1′-biphenyl]-4-yl)furan (4)

4-Bromobiphenyl (**3**) (4 mmol, 932 mg), 2-furanboronic acid (1.2 equiv., 560 mg), Pd[P(*t*-Bu_3)]$_2$ (2 mol%, 41 mg) and KF (900 mg) were dissolved in THF (10 mL) under nitrogen atmosphere. The mixture was stirred for 12 h at rt. The resulting mixture was poured into water and extracted by CH_2Cl_2. After concentration, the residue was purified by silica gel chromatography, giving the corresponding 2-([1,1′-biphenyl]-4-yl)furan (**4**) in 89% (780 mg) yield as a white solid. ^{1}H NMR (400 MHz, $CDCl_3$): δ 7.75 (d, 2H), 7.62 (d, 4H), 7.33–7.50 (m, 3H), 7.32–7.37 (m, 1H), 6.69 (d, 1H), 6.42–6.40 (m, 1H); ^{13}C NMR (100 MHz, $CDCl_3$): δ 153.62, 142.05, 140.48, 139.85, 129.75, 128.72, 128.71, 127.25, 126.81, 124.09, 111.67, 105.08.

Synthesis of BP2F

To a THF (45 mL) solution of 2-([1,1′-biphenyl]-4-yl)furan (**4**) (3 mmol, 670 mg) was added *n*-BuLi (1.57 M in *n*-hexane, 3 mmol, 1.92 mL) at −78 °C. After stirring for 0.5 h, the reaction mixture was warmed gradually to −40 °C. $CuCl_2$ (3 mmol, 420 mg) was added, and the mixture kept for 1 h at this temperature followed by warming to rt. After stirring at rt for 5 h, the mixture was filtered and the resulting residue was washed by water and MeOH. After sublimation at 310 °C, BP2F was obtained as a

yellow-green solid in 39% yield (260 mg). Anal. calcd for $C_{32}H_{22}O_2$: C 87.65, H 5.06, O 7.30; found: C 87.93, H 5.22%.

PVT method for preparation of single crystals and fabrication of single crystal OFET devices

BP2T, BPFT, and BP2F single crystals were grown by physical vapor transport in a stream of argon gas with a purity of 99.9999%. Pure powders of BP2T, BPFT, and BP2F (1–5 mg) were placed at the end of the tube on aluminum foil. After heating for 12 h, the good film-like crystals of BP2T and BPFT were obtained. The BP2F single crystal showed a needle-like shape. A highly doped silicon wafer with a 200 nm thermally grown SiO_2 layer was covered with a 60 nm thick film of PMMA by spin coating using toluene as solvent. The resulting film was annealed at 90 °C for 50 h in the glove box filled with argon gas. A thin crystal was laminated on this PMMA pretreated SiO_2 substrate. The top contact symmetric and asymmetric electrodes were realized by thermally evaporating gold and calcium metals through a shadow mask on top of the crystals. Electrical and optical characterizations were performed in the glove box under an inert Ar atmosphere by using a semiconductor parameter analyzer (Agilent Technology B1500A) and a CCD camera through an optical microscope. The observed light emission images were captured with a CCD camera.

Acknowledgements

This research was supported by the World Premier International Research Center Initiative (WPI), MEXT, Japan. We thank Prof. N. Kobayashi and Dr S. Shimizu at Tohoku University, Prof. T. Minato at Kyoto University, Prof. T. Matsuo at Kinki University, Dr T. Otani at Waseda University for their help with fluorescence measurements, Prof. N. Teramae and Prof. S. Nishizawa at Tohoku University for their help with thermal analysis measurements, and Dr E. Kwon at Tohoku University for X-ray single crystal analysis. Some of the calculations were performed using the supercomputing resources at Cyberscience Center, Tohoku University.

Notes and references

1 (*a*) O. Gidron, Y. Diskin-Posner and M. Bendikov, *J. Am. Chem. Soc.*, 2010, **132**, 2148; (*b*) U. H. F. Bunz, *Angew. Chem., Int. Ed.*, 2010, **49**, 5037; (*c*) G. R. Hutchison, M. A. Ratner and T. J. Marks, *J. Am. Chem. Soc.*, 2005, **127**, 16866; (*d*) J.-D. Huang, S.-H. Wen, W.-Q. Deng and K.-L. Han, *J. Phys. Chem. B*, 2011, **115**, 2140.

2 (*a*) Y. Miyata, T. Nishinaga and K. Komatsu, *J. Org. Chem.*, 2005, **70**, 1147; (*b*) Y. Miyata, M. Terayama, T. Minari, T. Nishinaga, T. Nemoto, S. Isoda and K. Komatsu, *Chem.–Asian J.*, 2007, **2**, 1492; (*c*) O. Gidron, A. Dadvand, Y. Sheynin, M. Bendikov and D. F. Perepichka, *Chem. Commun.*, 2011, **47**, 1976; (*d*) C. Mitsui, J. Soeda, K. Miwa, H. Tsuji, J. Takeya and E. Nakamura, *J. Am. Chem. Soc.*, 2012, **134**, 5448.

3 (*a*) C.-C. Wu, W.-Y. Hung, T.-L. Liu, L.-Z. Zhang and T.-Y. Luh, *J. Appl. Phys.*, 2003, **93**, 5465; (*b*) H. Tsuji, C. Mitsui, L. Ilies, Y. Sato and E. Nakamura, *J. Am. Chem. Soc.*, 2007, **129**, 11902; (*c*) H. Tsuji, C. Mitsui, Y. Sato and E. Nakamura, *Adv. Mater.*, 2009, **21**, 3776.

4 (*a*) C. H. Woo, P. M. Beaujuge, T. W. Holcombe, O. P. Lee and J. M. Fréchet, *J. Am. Chem. Soc.*, 2010, **132**, 15547; (*b*) P. M. Beaujuge and J. M. Fréchet, *J. Am. Chem. Soc.*, 2011, **133**, 20009; (*c*) A. T. Yiu, P. M. Beaujuge, O. P. Lee, C. H. Woo, M. F. Toney and J. M. Fréchet, *J. Am. Chem. Soc.*, 2012, **134**, 2180.

5 G. Distefano, D. Jones, M. Guerra, L. Favaretto, A. Modelli and G. Mengoli, *J. Phys. Chem.*, 1991, **95**, 9746.

6 (*a*) M. Muccini, *Nat. Mater.*, 2006, **5**, 605; (*b*) F. Cicoira and C. Santato, *Adv. Funct. Mater.*, 2007, **17**, 3421; (*c*) J. Zaumseil and H. Sirringhaus, *Chem. Rev.*, 2007, **107**, 1296.

7 (*a*) A. Hepp, H. Heil, W. Weise, M. Ahles, R. Schmechel and H. von Seggern, *Phys. Rev. Lett.*, 2003, **91**, 157406; (*b*) T. Takahashi, T. Takenobu, J. Takeya and Y. Iwasa, *Adv. Funct. Mater.*, 2007, **17**, 1623; (*c*) H. Nakanotani, R. Kabe, M. Yahiro, T. Takenobu, Y. Iwasa and C. Adachi, *Appl. Phys. Express*, 2008, **1**, 091801; (*d*) T. Takenobu, S. Z. Bisri, T. Takahashi, M. Yahiro, C. Adachi and Y. Iwasa, *Phys. Rev. Lett.*, 2008, **100**, 066601; (*e*) Y. Wang, R. Kumashiro, R. Nouchi, N. Komatsu and K. Tanigaki, *J. Appl. Phys.*, 2009, **105**, 124912; (*f*) Y. Wang, D. Liu, S. Ikeda, R. Kumashiro, R. Nouchi, Y. Xu, H. Shang, Y. Ma and K. Tanigaki, *Appl. Phys. Lett.*, 2010, **97**, 033305; (*g*) R. Capelli, S. Toffanin, G. Generali, H. Usta, A. Facchetti and M. Muccini, *Nat. Mater.*, 2010, **8**, 496; (*h*) S. Z. Bisri, T. Takenobu, K. Sawabe, S. Tsuda, Y. Yomogida, T. Yamao, S. Hotta, C. Adachi and Y. Iwasa, *Adv. Mater.*, 2011, **23**, 2753; (*i*) M. Melucci, L. Favaretto, M. Zambianchi, M. Durso, M. Gazzano, A. Zanelli, M. Monari, M. G. Lobello, F. De Angelis, V. Biondo, G. Generali, S. Troisi, W. Koopman, S. Toffanin, R. Capelli and M. Muccini, *Chem. Mater.*, 2013, **25**, 668.

8 A. Dadvand, A. G. Moiseev, K. Sawabe, W.-H. Sun, B. Djukic, I. Chung, T. Takenobu, F. Rosei and D. F. Perepichka, *Angew. Chem., Int. Ed.*, 2012, **51**, 3837.

9 (*a*) S. Z. Bisri, T. Takenobu, Y. Yomogida, H. Shimotani, T. Yamao, S. Hotta and Y. Iwasa, *Adv. Funct. Mater.*, 2009, **19**, 1728; (*b*) Y. Wang, R. Kumashiro, Z. Li, R. Nouchi and K. Tanigaki, *Appl. Phys. Lett.*, 2009, **95**, 103306.

10 (*a*) M. B. Smith and J. Michl, *Chem. Rev.*, 2010, **110**, 6891; (*b*) P. M. Zimmerman, F. Bell, D. Casanova and M. Head-Gordon, *J. Am. Chem. Soc.*, 2011, **133**, 19944.

11 (*a*) S. Varghese and S. Das, *J. Phys. Chem. Lett.*, 2011, **2**, 863; (*b*) P. Katoh, K. Suzuki, A. Furube, M. Kotani and K. Tokumura, *J. Phys. Chem. C*, 2009, **113**, 2961.

12 CCDC 922141 (BP2F) and 922142 (BPFT) contain the supplementary crystallographic data for this paper.†

13 S. Hotta, M. Goto, R. Azumi, M. Inoue, M. Ichikawa and Y. Taniguchi, *Chem. Mater.*, 2004, **16**, 237.

14 The detailed theoretical study for BPFT aggregates including excitation energy and transition dipole moment, see: H. Tamura, I. Hamada, H. Shang, K. Oniwa, M. Akhtaruzzaman, T. Jin, N. Asao, Y. Yamamoto,

K. Thangavel, H. Shimotani, S. Ikeda and K. Tanigaki, *J. Phys. Chem. C*, 2013, **117**, 8072.

15 The transfer integrals were calculated using the PW91/QZ4P level of DFT implemented in the Amsterdam density functional (ADF) program, see: G. Te Velde, F. M. Bickelhaupt, E. J. Baerends, C. Fonseca Guerra, S. J. A. Van Gisbergen, J. G. Snijders and T. Ziegler, *J. Comput. Chem.*, 2001, **22**, 931.

